Coupling of Surface-Plasmon-Polariton-Hybridized Cavity Modes between Submicron Slits in a Thin Gold Film

R. Walther,[§,*] *S. Fritz,*[§] *E. Müller,*[§] *R. Schneider,*[§] *D. Gerthsen,*[§] *W. Sigle,*[†] *T. Maniv,*[#] *H. Cohen,*[♦] *C. Matyssek,*[◊] *K. Busch*[◊,♣]

[§]Laboratorium für Elektronenmikroskopie, Karlsruher Institut für Technologie (KIT), 76128 Karlsruhe, Germany

[†] Max-Planck-Institut für Festkörperforschung, 70569 Stuttgart, Germany

[#]Schulich Faculty of Chemistry, Technion – Israel Institute of Technology, Haifa 32000, Israel

[♦]Department of Chemical Research Support, Weizmann Institute of Science, Rehovot 76100, Israel

[◊]Humboldt-Universität zu Berlin, Institut für Physik, AG Theoretische Optik & Photonik, 12489 Berlin, Germany

[♣]Max-Born-Institut, 12489 Berlin, Germany

Supporting Information

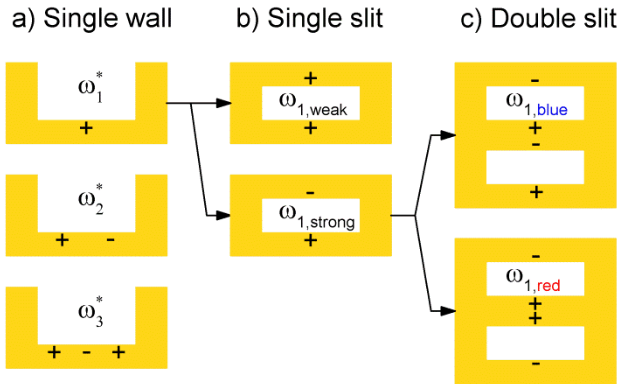

Figure S1. Localized surface plasmon modes supported by a) a single wall (i.e. a slit with infinite width), b) a single slit, and c) a 2-slit system. The charge distributions of the respective modes are marked by +/-. The Figure is adapted from the work of Ögüt et al.[1]

Figure S1 shows the relevant possible localized surface plasmon modes for our work. Starting with a single wall with a finite extension corresponding to the slit length in Figure S1a, the fundamental, the 2nd, and 3rd harmonic modes are indicated by their charge distributions. The fundamental has only one anti-node at the wall center whereas the 2nd and 3rd harmonics have two and three anti-nodes as expected from standing-wave like cavity modes. In contrast to nanorods, there is always a node at the wall edges.

If a second wall is close, i.e. a single slit is formed; the SPPs on either wall hybridize as shown in Figure S1b. This leads to the formation of two possible modes with symmetric (top slit) and antisymmetric (bottom slit) SPPs on the walls, denoted by $\omega_{1,weak}$ and $\omega_{1,strong}$, respectively. The latter one results in a strong electric field within the slit as opposite charges face each other. Therefore, this mode appears with a higher intensity in EEL spectra. For $\omega_{1,weak}$ on the other hand, repelling charges are located on the opposite walls which leads to a weak electric field and consequently also a lower intensity in EEL spectra. The hybridization also leads to energy shifts, i.e. the anti-symmetric mode has reduced energy and the symmetric mode increased energy. For the sake of simplicity we denoted $\omega_{1,strong}$ as the fundamental mode in our manuscript as $\omega_{1,weak}$ is barely observed in the spectra and cannot be analyzed in detail.

If two single slits are in close proximity to each other, further hybridizations occur as depicted in Figure S1c. Only the two possible hybridizations of $\omega_{1,strong}$ are depicted. The electric field in the slits is now taken into account to define anti-symmetric and symmetric modes. In the top 2-slit system, the fields in both slits have the same direction leading to the symmetric mode. This mode corresponds to the higher-energy mode which is the blue-shifted branch of the fundamental, i.e. $\omega_{1,blue}$. The anti-symmetric mode corresponds to the low-energy mode and is thus denoted as $\omega_{1,red}$. The depicted charge distributions can also be used to explain the observed intensity variations of the modes. For $\omega_{1,red}$, identical charges are located on both walls of the metal bar. This leads to constructive interference with doubled amplitude and hence four-times the intensity as seen in Figure 5b for $d/L < 0.2$. On the other hand, for $\omega_{1,blue}$, opposite charges are located on the metal bar and hence destructive interference occurs and the mode is barely excited (cf. Figure 5b). However, this argumentation only holds for small inter-slit distances. For large ones, the SPPs on either side of the metal bar are too distant to interact.

Deconvolution with the Richardson-Lucy algorithm

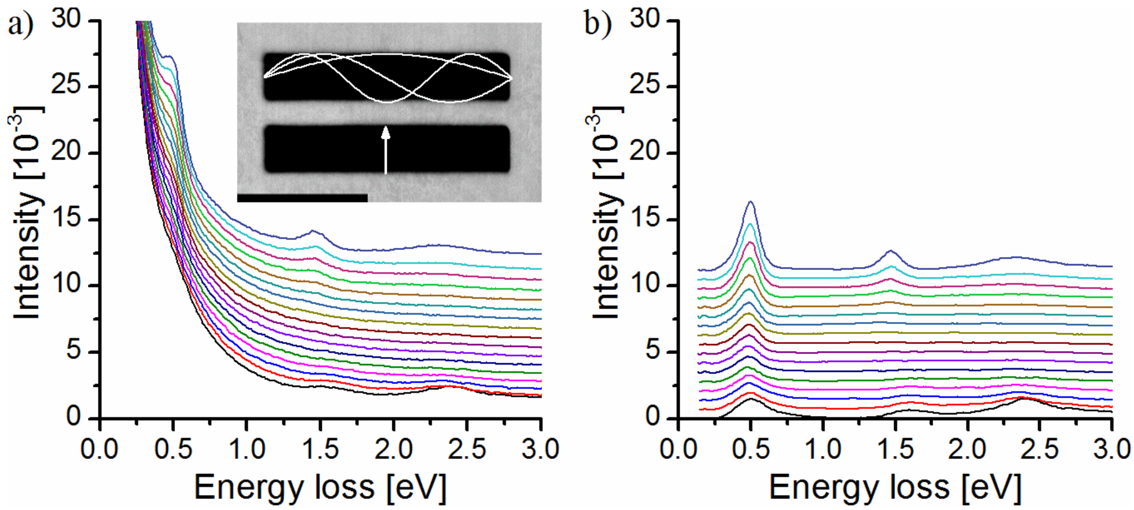

Figure S2. a) EELS spectra taken along a line across the first slit in a double-slit system. The slits have a size of 960 nm x 180 nm and are separated by a metal bar with 100 nm width. The fundamental cavity mode and its third harmonic are enhanced when the central metal bar is approached. The inset shows an HAADF STEM image of the double-slit system. The arrow depicts the scan direction and the back scale bar corresponds to 500 nm. The first 3 cavity modes are indicated schematically in the upper slit. b) The same series of spectra after applying seven iterations with the RL algorithm and subsequent background subtraction. The fundamental mode is now clearly observed at the outer slit wall (black spectrum).

In the following we demonstrate the application of the Richardson-Lucy (RL) algorithm[2, 3] and demonstrate that seven iterations with the RL algorithm allow to extract quantitative signal intensities from EEL spectra.

Figure S2 shows EELS spectra of a transversal scan performed across one slit in a 2-slit system with a slit length L = 960 nm. The spectra were acquired along a line at $L/2$ as indicated by the white arrow in the high-angle annular dark-field scanning transmission electron microscopy (HAADF STEM) image of the 2-slit system (inset Figure S2a). To illustrate the difficulties encountered when low-energy signals are to be extracted, raw spectra and spectra after processing with the RL algorithm and background subtraction are shown in Figures. S2a,b. Close to the outer wall of the 2-slit system, the raw EELS spectrum (black line in Figure S2a) only shows the Au surface plasmon at an energy loss ΔE = 2.3eV and a weak signal at about 1.5 eV. Moving across the slit, another signal at 0.5 eV emerges and the intensity of the 1.5 eV signal increases substantially. As demonstrated by Carmeli et al[4]., the electron beam interacts with the metal wall over long distances by exchanging photons within the light cone over several 100 nm. This leads to the excitation of SPPs and an associated cavity standing wave which are revealed by weak signals in the EELS spectrum well below the Au surface plasmon of the extended Au film. The signals at ΔE = 0.5 eV and 1.5 eV are related to the fundamental mode ω_1 and third harmonic ω_3 of the cavity standing wave which are excited along the 960 nm axis of the slit as schematically indicated in the HAADF STEM image (Figure S2a). These two modes are at maximum intensity at $L/2$.

In the following we will focus on the test of the RL algorithm which is essential to extend the detectability of weak low-energy signals and the extraction of quantitative intensity information. Considering the raw spectra (Figure S2a), the signal at ΔE = 0.5 eV is only visible close to the central metal bar and cannot be recognized in the tail of the ZLP close to the outer slit wall. Background fitting by an exponential function does not reliably recover this weak signal. Subtraction of a scaled reference spectrum obtained without specimen can give reasonable results under favorable circumstances if the FWHM of the reference spectrum exactly agrees with the spectrum to be evaluated. Other standard zero-loss removal procedures, e.g., in the Gatan Digital Micrograph software were tested but were not suited to produce reliable results. Figure S2b shows the same spectra after seven iterations with the RL algorithm and subsequent background subtraction with a bi-exponential function which clearly reveal the 0.5 eV signal and its intensity increase towards the central metal bar.

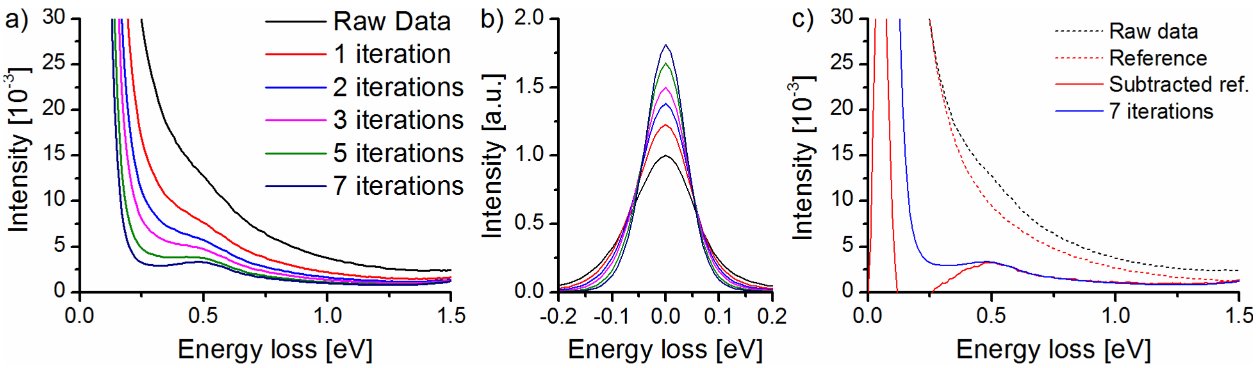

Figure S3. a) Spectra for energy losses below 1.5 eV showing the tail of the ZLP after up to seven iterations with the RL algorithm. The raw spectrum was recorded at 20 nm distance to the outer slit wall. b) Sharpening on the ZLP and c) detailed analysis of the spectra depicted in a). Shown are the raw spectrum (black dashed line), a vacuum reference spectrum (red dashed line), spectrum after seven iterations with the RL algorithm (solid blue line) and the raw data after reference subtraction (solid red line).

Signal processing and iteration numbers n with the RL algorithm need to be carefully tested with respect to quantification of the signal intensity. Figure S3a shows the evolution of a raw spectrum (black line in Figure S3a) taken at 20 nm distance to the outer slit wall for an increasing number n of iterative applications with the RL algorithm. The raw spectrum only shows a weak shoulder at ΔE = 0.5 eV that evolves into a discernible signal already for small n. For more than five iterations, the resolution improvement (observable as a shift of the tail of the ZLP to the left) clearly detaches the ZLP from the SPP signal. Figure S3b shows the evolution of the ZLP with increasing n. The ZLP is sharpened under conservation of the total number of counts which leads to the reduction of the FWHM of the ZLP from typically 0.11 eV to 0.07 eV and a corresponding height increase. For $n > 5$ the ZLP becomes edgy due to the sampling with 0.01 eV per channel, which poses a limit to the achievable enhancement of the energy resolution in this case. The influence of the RL algorithm on the spectrum is reduced for increasing energy losses ΔE. For $\Delta E > 1.5$ eV these few iterations barely change the spectrum apart from lowering the intensity compared to the raw spectrum. For a small number of iterations, the RL algorithm mainly reduces the FWHM and tail of the ZLP. It is crucial that sharpened data is not again normalized with respect to the ZLP height because the RL algorithm conserves the total number of counts in the spectrum. Normalization with respect to the ZLP height after sharpening would lead to reduced signal intensities in the processed spectrum. Figure S3c compares spectra after processing with the RL algorithm (n = 7) (blue line) and after subtraction of a vacuum reference spectrum (solid red line).

Beyond 0.5 eV the RL-processed spectrum coincides with the reference-subtracted spectrum but there are differences at lower Δ*E*. As the FWHM of the reference spectrum is even slightly broader than the spectrum recorded from the slit structure, a dip in intensity at ΔE < 0.5 eV occurs. Quantification of signal intensity after reference subtraction may give an artificially reduced intensity of the 0.5 eV signal. On the other hand, it is not yet obvious from these considerations whether the correct spectrum is retrieved after seven iterations.

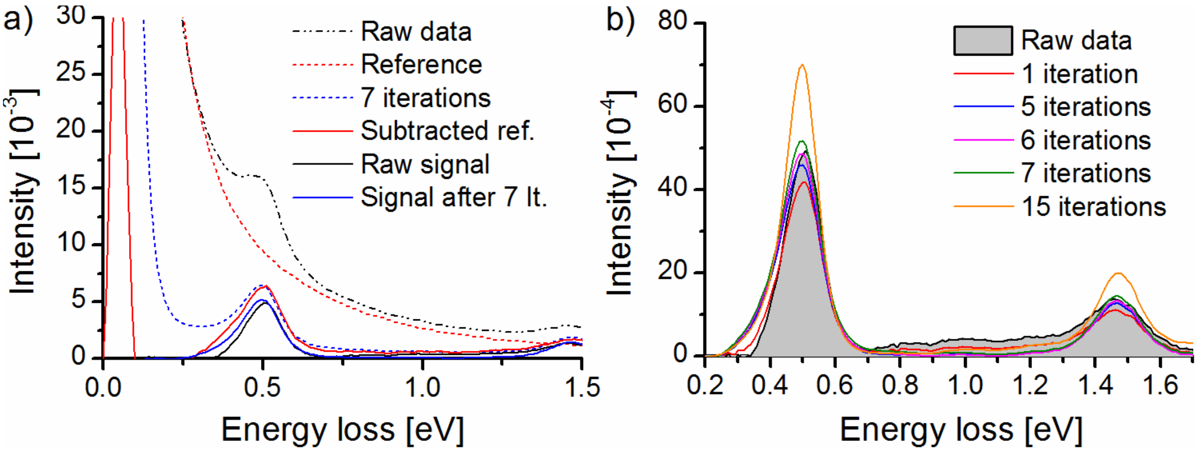

Figure S4. a) Illustration of different processing methods of a spectrum taken at 10 nm distance from the metal bar (see legend for spectra denotations). b) Background-subtracted spectra after up to 15 iterations with the RL algorithm.

To check the effect of the RL algorithm we applied the same procedure to a spectrum acquired at 10 nm distance from the central metal bar of the two-slit system (Figure S4a). Here, the intensity of the 0.5 eV signal is comparatively high in the raw spectrum (black dash-dotted line). Figure S4a also contains a reference spectrum (red dashed line) and the raw spectrum after seven iterations with the RL algorithm (blue dashed line). The real intensity of the 0.5 eV signal can be well extracted from the background-subtracted raw spectrum (solid black line) due to the high signal intensity. This spectrum agrees well with the RL-processed data (solid blue line) after background subtraction and 7 iterations. The intensity of the reference-subtracted spectrum (solid red line) is slightly higher. This can be understood by the FWHM of the ZLP of the reference spectrum which slightly differs from the raw spectrum. To investigate effect of the iteration number with respect to quantification of the signal intensity, up to 15 iterations with the RL algorithm were applied to a raw spectrum which contains the 0.5 eV signal with a high intensity. Figure S4b shows the resulting signal intensities at ΔE ≈ 0.5 eV after background subtraction. The signal for the unsharpened spectrum (raw data after background subtraction) is highlighted (grey filling) for better visibility and comparison with the RL-processed data. A reduced signal intensity is observed for a small number of iterations ($n \leq 3$). The signal intensity increases with n and agrees well with the peak intensity of the raw data for $5 \leq n \leq 7$. Larger n values further increase the peak height due to peak sharpening. A small number of iterations only have a strong effect on the ZLP tail (cf. Figure S3a) which leads to an improved visibility of low-energy signals without altering them significantly. The same observation is made for the third harmonic of the cavity mode (cf. Figure S4b). Finally, it is noted that the optimum number of iteration may differ, depending on the acquisition conditions, and has to be individually determined.

References

1. Ögüt, B.; Vogelgesang, R.; Sigle, W.; Talebi, N.; Koch, C. T.; van Aken, P. A. Hybridized metal slit eigenmodes as an illustration of Babinet's principle. *ACS Nano* **2011**, 5, 6701-6.

2. Zuo, J. M. Electron detection characteristics of a slow-scan CCD camera, imaging plates and film, and electron image restoration. *Microsc. Res. Tech.* **2000**, 49, 245-68.

3. Gloter, A.; Douiri, A.; Tence, M.; Colliex, C. Improving energy resolution of EELS spectra: an alternative to the monochromator solution. *Ultramicroscopy* **2003**, 96, 385-400.

4. Carmeli, I.; Itskovsky, M. A.; Kauffmann, Y.; Shaked, Y.; Richter, S.; Maniv, T.; Cohen, H. Far- and near-field electron beam detection of hybrid cavity-plasmonic modes in gold microholes. *Phys. Rev. B* **2012**, 85, 041405-5.